Diagnosing the Impact of Stratospheric Planetary Wave Breaking in a Linear Model

CHRISTIAN HAUCK* AND VOLKMAR WIRTH

Meteorologisches Institut, Universität München, Munich, Germany

(Manuscript received 10 March 2000, in final form 17 October 2000)

ABSTRACT

In the past, linear quasigeostrophic theory has proven successful in modeling the vertical and meridional propagation of stationary planetary waves in the stratosphere. Since in such models the wave solution does not sensitively depend on the wave damping, the latter was usually implemented as relaxation with a simple damping coefficient. As far as the damping is concerned, this is likely to be unrealistic, since it does not account for the locally enhanced dissipation arising from stratospheric Rossby wave breaking. In the present study, a parameterization for Rossby wave breaking (Garcia) is applied to obtain an improved representation of wave damping throughout the stratosphere. Although solving for the wave turns into a nonlinear problem, the model remains linear in the sense that both the basic-state zonal wind and the wave at the tropopause level are specified and kept fixed. The divergence of the Eliassen–Palm flux and the steady-state residual circulation are computed in order to diagnose the impact of the waves on the mean flow. Both quantities depend sensitively and in a complex manner on the given basic-state zonal flow. The model is applied to different scenarios representing the different phases of an idealized quasi-biennial oscillation (QBO). The dependence of the wave forcing on the phase of the QBO is consistent with results from previous studies. The current model allows a clear attribution of differences in wave–mean-flow interaction to differences in the basic flow.

1. Introduction

Linear quasigeostrophic theory on a hemisphere has sucessfully been applied to describe the vertical and meridional propagation of quasistationary planetary waves in the stratosphere (e.g., Matsuno 1970, 1971; Karoly and Hoskins 1982; Wirth 1991; Braesicke 1994). The model was first formulated by Matsuno (1970). Given a zonal mean basic state and some forcing at the tropopause level, Matsuno's model yields the wave structure throughout the stratosphere. Overall, the wave disturbances thus calculated turn out to be in qualitative agreement with observations. Moreover, the so-called refractive index has proven to be a helpful diagnostic for interpreting the strength and pattern of the wave in terms of the basic state.

The success of Matsuno's model is based on its ability to simulate Rossby wave propagation in a qualitatively realistic manner. On the other hand, it is not straightforward to extract meaningful information from this model about the interaction between the waves and the mean flow. Obviously, since the model is linear, it does not explicitly describe wave mean–flow interaction. Yet, there are ways to diagnose the latter indirectly. The current paper suggests a new method, which allows one to gain useful information about the impact of the waves on the mean flow in the context of Matsuno's model.

A key diagnostic for wave–mean-flow interaction is the divergence of the Eliassen–Palm (EP) flux $\mathbf{F}$ (Charney and Drazin 1961; Andrews and McIntyre 1976, 1978; Andrews et al. 1987). The waves interact with the mean flow to the degree that $\nabla \cdot \mathbf{F}$ deviates from zero. In the case of strictly conservative conditions, $\nabla \cdot \mathbf{F}$ is zero for stationary linear waves on a purely zonal basic state. However, in most applications of Matsuno's model, some small but nonzero wave damping is included through simple relaxation of the perturbation potential vorticity q' toward zero, with a damping coefficient α. This is physically motivated because real waves are damped by nonconservative processes; at the same time, it prevents the mathematical singularity of linear theory at the critical lines, that is, at those locations where the basic-state zonal flow vanishes. Since the wave amplitude, which was the focus of most previous studies, does not sensitively depend on the damping coefficient (e.g., Wirth 1991), the specification of α

* Current affiliation: Laboratory of Hydraulics, Hydrology and Glaciology, Swiss Federal Institute of Technology, Zurich, Switzerland.

Corresponding author address: Volkmar Wirth, Institute for Physics of the Atmosphere, University of Mainz, Becherweg 21, 55099 Mainz, Germany.
E-mail: vwirth@mail.uni-mainz.de

was usually not considered to be very important, and α was chosen to be a constant or a simple function of altitude. The inclusion of wave damping in Matsuno's model renders the divergence of the EP flux nonzero. Strictly speaking, the thus calculated field of $\nabla \cdot \mathbf{F}$ can be considered to be a diagnostic for wave mean–flow interaction, but it is not clear a priori whether this is realistic at all.

In the present paper, we show that, indeed, through a careful design of the damping coefficient α, the divergence of the EP flux can be made qualitatively realistic, thus allowing a meaningful interpretation of the effect of the wave on the mean flow. To this end, it turns out to be essential to account for Rossby wave breaking. Although this process is rather localized, it can make a significant contribution to the damping of the waves (McIntyre and Palmer 1984).

We locally modify the damping coefficient by implementing a parameterization of Rossby wave breaking that has been developed by Garcia (1991). Previous studies have shown that this parameterization yields a fairly realistic representation of wave damping, especially near critical lines, where planetary waves tend to break vigorously. In the original paper, Garcia tested his parameterization in a numerical model, which includes governing equations for both a single wave and the zonal-mean flow. There was remarkable agreement between the calculations and corresponding observations. Later, Randel and Garcia (1994) applied the parameterization to 12 yr of stratospheric circulation statistics; the damping rates thus obtained were in good agreement with the parameterized calculations of Garcia (1991).

The present study differs from previous work in that it applies Garcia's parameterization in the framework of a Matsuno-type model. The model is linear in the sense that both the basic state zonal wind and the wave at the tropopause level are given and held fixed. Nevertheless, owing to Garcia's parameterization solving for the wave turns into a nonlinear problem. Its solution will be obtained through iteration. From this, we compute the divergence of the EP flux and the steady-state residual circulation in order to quantify the wave forcing on the mean flow. It will be shown that these diagnostic quantities depend nonlinearly on the lower boundary forcing and are sensitive to small changes of the basic-state zonal wind.

In order to demonstrate the diagnostic power of this new approach, we will apply our model to a scenario in which wave mean–flow interaction is known to play an important role. We consider the relationship between the quasi-biennial oscillation (QBO) and the strength of the polar vortex (Holton and Tan 1980, 1982; Labitzke 1982, 1987; van Loon and Labitzke 1987; Dunkerton and Baldwin 1991; Kodera 1991; Palmer 1981a,b; Robinson 1986). Our results are qualitatively consistent with the results from previous investigations. The current work throws new light on the issue, since it allows us to quantitatively attribute the differences in wave forcing between the phases of the QBO to small differences in the basic flow. Moreover it facilitates the distinction between wave propagation and wave dissipation.

The paper is organized as follows. Section 2 describes how we implemented Garcia's parameterization in the framework of Matsuno's model. The impact of the wave breaking parameterization on the EP flux divergence and the diagnosed residual circulation is demonstrated in section 3. In section 4, we illustrate the model performace by considering different basic states corresponding to the different phases of an idealized QBO. Finally, a summary and conclusions are provided in section 5.

2. The modified Matsuno model

Our model is standard in every respect except for the treatment of the wave damping. Denoting the zonally symmetric basic state by an overbar and the deviation therefrom by a prime, the linearized equation for the quasigeostrophic potential vorticity q (henceforth abbreviated as PV) in hemispheric geometry can be written as

$$\left(\frac{\partial}{\partial t} + \frac{\overline{u}}{a\cos\phi}\frac{\partial}{\partial\lambda}\right)q' + a^{-1}\overline{q}_{\phi}v' = -\alpha q', \qquad (1)$$

where $\overline{u}$ is the basic-state zonal wind, v' is the perturbation meridional wind, α is the damping coefficient, and a denotes the radius of the earth (e.g., Andrews et al. 1987). The coordinates are longitude λ, latitude ϕ, and log-p-altitude z with scale height H. A coordinate as a subscript denotes the partial derivative with respect to that coordinate.

Restricting attention to stationary wave solutions of wavenumber s and expressing the perturbation quantities in (1) through the perturbation geopotential

$$\Phi'(\lambda, \phi, z) = e^{z/(2H)}\,\mathrm{Re}\hat{\Psi}(\phi, z)e^{is\lambda}, \qquad (2)$$

reduces (1) to a partial differential equation for $\hat{\Psi}(\phi, z)$, which symbolically can be written as

$$\mathcal{L}\hat{\Psi} + n_s^2\hat{\Psi} = 0. \qquad (3)$$

Here, $\mathcal{L}$ is an elliptic second-order differential operator, and n_s^2 is the so-called refractive index squared (see Andrews et al. 1987).

The system is forced by specifying the wave Φ'_{TP} at the tropopause level, that is, at the lower boundary of the domain, which in our case is at 200 hPa. On the other boundaries, Φ' is set to zero. In order to suppress spurious reflexions, sponge layers are added close to the upper and equatorial boundary, as described in Wirth (1991). As reference basic state, we take the Northern Hemisphere January climatology from Randel (1992), shown in Fig. 1 together with the corresponding meridional potential vorticity gradient $\overline{q}_{\phi}$. This basic state will be used to quantify the impact of the wave breaking on the model results in section 3, and suitable modifications to it will serve to illustrate the model performance in section 4. The model domain is chosen to be

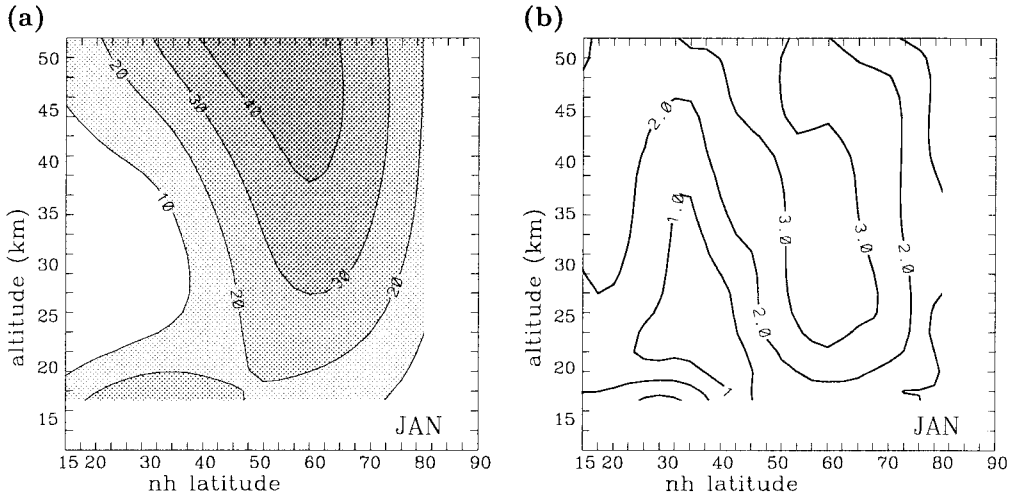

FIG. 1. Jan climatology, which is used as basic state. (a) Zonal mean zonal wind $\overline{u}$ (in m s^{-1}, contours every 10 m s^{-1}); (b) meridional potential vorticity gradient $\overline{q}_\phi$ (in 10^{-11} s^{-1}). The wind data are taken from Randel (1992).

the Northern Hemisphere stratosphere between 15° and 90°N and between 12 and 50 km altitude. The number of grid points is 33×33, corresponding to a horizontal grid spacing of 2.5° in the meridional direction and 1.67 km in the vertical. We found that the use of higher spatial resolution does not affect our results significantly. Equation (3) is solved numerically with the help of a direct solver (Lindzen and Kuo 1969).

The nonconservative processes are modeled through linear relaxation, as formulated on the right-hand side of (1). The damping coefficient α is our key quantity. It is written as the sum of two parts,

$$\alpha(\phi, z) = \alpha_0(z) + \delta(\phi, z). \tag{4}$$

The first part $\alpha_0(z)$ is specified as in Wirth (1991), increasing linearly from 0.05 to 0.2 day^{-1} between 20 and 50 km. Similar damping has been used in numerous previous studies. It assumes that dissipation of both momentum and temperature has a relaxational character with the same relaxation timescale. This can be considered to give a broad representation of global nonconservative processes. On the other hand, it certainly fails to give a realistic representation of the damping due to planetary wave breaking, which can be large locally, but which is typically limited to restricted areas in the meridional plane. In order to account for the wave breaking, we follow Garcia's suggestion using linear relaxation with a suitably defined local damping rate $\delta(\phi, z)$.

Garcia's parameterization is based on concepts similar to those developed by Lindzen (1981) for the parameterization of gravity wave breaking. While the underlying mechanism is convective instability in the case of gravity wave breaking, it is associated with barotropic and baroclinic instability in the present case. Regions of planetary wave breaking are identified as those regions where

$$R = |q'_\phi|/\overline{q}_\phi \geq 1. \tag{5}$$

The coefficient δ is zero except where (5) is satisfied. There, it is made large enough such that further wave growth is prevented. The magnitude of δ, which renders the waves marginally stable, is obtained by constraining the equation for the Rossby wave activity A (see Andrews et al. 1987),

$$\nabla \cdot (\mathbf{c}_g A) = -2\delta A, \tag{6}$$

with the condition for wave saturation, $R = 1$. Here, $\mathbf{c}_g$ represents the group velocity based on the local wavenumbers l and m in the meridional and vertical direction, respectively. Making explicit use of the WKBJ dispersion relation for planetary waves, one can derive the following expression for the damping rate:

$$\delta \equiv \delta[\Phi', \overline{u}] = \frac{2kl}{K^2}\left[-\frac{5}{3a}\overline{u}_\phi\right] + \frac{2k\epsilon m}{K^2}\left[\frac{\overline{u}}{2H} - \frac{3}{4}\overline{u}_z\right], \tag{7}$$

where $k = 2\pi s/(a\cos\phi)$, $\epsilon = (f/N)^2$, f is the Coriolis parameter, N the log pressure boyancy frequency, and $K^2 = k^2 + l^2 + \epsilon(m^2 + 0.25/H^2)$. For details, the reader is referred to Garcia (1991).

As indicated in (7), the coefficient δ depends both on the basic state (via $\overline{u}$) and on the wave (via the local wavenumbers l and m). It follows that equation (1) with $\alpha = \alpha_0 + \delta$ is nonlinear in the perturbation quantity. It is solved iteratively by carrying out the following steps.

1) Equation (3) is solved with $\alpha = \alpha_0(z)$.
2) The wave solution obtained in the previous step is used to compute the local wavenumbers l and m (see Garcia 1991) and to determine the regions of wave breaking [i.e., those regions where (5) is satisfied].
3) The coefficient δ is computed from (7) in the regions

of wave breaking; in the other regions, δ is set to zero.

4) Equation (3) is solved for a new wave with $\alpha = \alpha_0(z) + \delta(\phi, z)$, where δ is the field computed in the previous step.

Steps 2 to 4 are repeated until convergence. Details about the convergence can be found in the appendix.

The EP flux divergence for wavenumber s is

$$\nabla \cdot \mathbf{F} = \frac{1}{a\cos\phi}\frac{\partial}{\partial\phi}(\cos\phi F^{(\phi)}) + \frac{\partial F^{(z)}}{\partial z}, \quad (8)$$

with the EP flux given by

$$\mathbf{F} \equiv (0, F^{(\phi)}, F^{(z)}) = \frac{1}{2}\rho_0 s A_s^2\left(0, \frac{1}{f^2 a}\frac{\partial\chi_s}{\partial\phi}, \frac{1}{N^2}\frac{\partial\chi_s}{\partial z}\right). \quad (9)$$

Here, $A_s(\phi, z)$ and $\chi_s(\phi, z)$ denote the amplitude and phase of wave s, respectively, and ρ_0 is the density in log pressure space (Andrews et al. 1987). As noted before, $\nabla \cdot \mathbf{F}$ is a measure for the impact of the wave on the zonal mean flow. This can most clearly be seen in the transformed Eulerian-mean (TEM) formalism, where the equation for the zonal mean wind reads

$$\frac{\partial\overline{u}}{\partial t} - f\overline{v}^* - \overline{X} = D_F, \quad (10)$$

with

$$D_F \equiv \frac{\nabla \cdot \mathbf{F}}{\rho_0 a\cos\phi}, \quad (11)$$

(Andrews et al. 1987). Here, $\overline{v}^*$ is the residual meridional wind, and $\overline{X}$ designates a zonal mean drag term. The quantity D_F, which is a scaled version of $\nabla \cdot \mathbf{F}$, will be called ''wave forcing'' in the following; it should not be confused with the ''forcing'' Φ'_{TP}, which is the wave specifed at the lower boundary of the domain. In general, nonzero wave forcing D_F in (10) is balanced partly by a local change of the zonal mean wind and partly by a nonvanishing residual circulation. The latter results in nonlocal effects even in the event of very localized D_F. We express the residual circulation $(\overline{v}^*, \overline{w}^*)$ in terms of a streamfunction ψ according to

$$(\rho_0\cos\phi\,\overline{v}^*, \rho_0\cos\phi\,\overline{w}^*) = (-\psi_z, a^{-1}\psi_\phi). \quad (12)$$

In the stationary limit and with $\overline{X} = 0$, (10) reduces to a balance between the Coriolis term $f\overline{v}^*$ and the wave forcing D_F. The corresponding streamfunction is given by

$$\psi(\phi, z) = -\frac{\cos\phi}{2\Omega\sin\phi}\int_z^\infty \rho_0(z')D_F(z', \phi)\,dz', \quad (13)$$

(''downward control principle'') (see Haynes et al. 1991; Holton et al. 1995). For the actual computation, we evaluate the integral in (13) with the upper boundary of the integration located close to the upper boundary of the domain just below the onset of the sponge layer.

The two quantities, D_F from (11) and ψ from (13), are considered to be our diagnostic tools for quantifying the wave forcing and its nonlocal effect. As main application we envisage the investigation of different lower boundary forcings Φ'_{TP} and different basic states $\overline{u}$, trying to find out how the amplitude of Φ'_{TP} and small differences in $\overline{u}$ affect D_F and ψ.

3. Model performance

We consider zonal wavenumber 1 and the reference basic state shown in Fig. 1. At the lower boundary, we specify Φ'_{TP}, corresponding to the Northern Hemisphere January climatology at 200 hPa taken from Randel (1987). First, the model is run with $\alpha = \alpha_0$; in this mode, it is equivalent to the standard Matsuno model. Using the wave solution from (1), a damping coefficient δ_0 is calculated from (7) in those regions where (5) is satisfied. The result is shown in Fig. 2a. Here, the grey shading indicates areas of substantial damping, and the steps in the shading are at 0.05, 0.15, 0.25, and 0.35 day^{-1}, respectively, which is equivalent to a characteristic damping time $\tau \equiv \delta_0^{-1}$ of 20, 7, 4, and 3 days. The quantity δ_0 in Fig. 2a is equivalent to our damping coefficient δ before the iteration is carried out. We then let the iteration go, computing alternating solutions for Φ' and δ. The coefficient δ obtained after final convergence is shown in Fig. 2b. Comparison of Figs. 2a and 2b demonstrates a nontrivial change of δ during the iteration, indicating substantial nonlinearity of our model equation associated with the wave breaking parameterization.

The final damping rate δ in Fig. 2b has a maximum value of about 0.3 day^{-1}, corresponding to a characteristic damping time $\tau \equiv \delta^{-1}$ of approximately 3 days. This is in good agreement with the results of Garcia (1991), who explicitly accounted for the feedback between the waves and the basic state and who obtained damping rates between 0.2 and 0.4 day^{-1}. Similar values were found by Randel and Garcia (1994), who applied the parameterization to observational data. In order to clearly identify the relative location of regions with enhanced damping with respect to the basic state, the latter is depicted by the dashed contours in Fig. 2 (cf. Fig. 1a). Apparently, the major portion of the damping occurs on the equatorward flank of the polar night jet. There is also some damping on its poleward flank, but the jet core is a region of very weak damping. This pattern and its relation with respect to the polar night jet turned out to be a robust feature, provided that there is significant wave breaking at all. Moreover, it is consistent with the results from previous studies, which used the same or a similar wave breaking parameterization (Garcia 1991; Randel and Garcia 1994; Kinnersley 1995).

In order to demonstrate the impact of the additional damping δ more explicitly, Fig. 3 presents a comparison between a model run with the wave breaking parameterization and a model run without this parameterization. In terms of wave amplitude (upper row), there is hardly

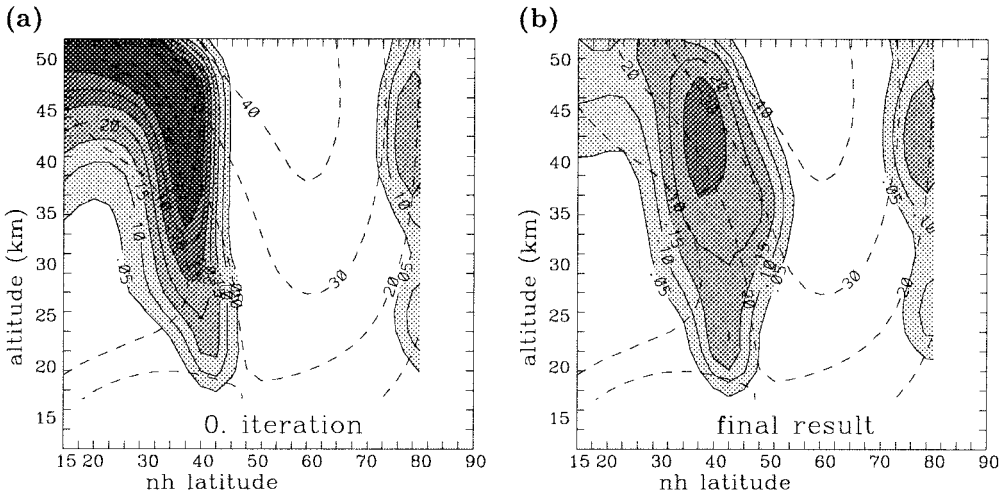

FIG. 2. Damping rates δ_0 and δ, respectively, (shading, in day^{-1}, steps in gray shading at 0.05, 0.15, 0.25, and 0.35 day^{-1}) and basic state zonal wind $\bar{u}$ (in m s^{-1}, dashed, contours every 10 m s^{-1}) for the reference basic state and wavenumber 1. The quantity δ_0 in (a) corresponds to the field δ before the iteration is carried out, while δ in (b) is the field to which the iteration finally converges.

any difference between the two runs. This is consistent with previous studies, indicating weak sensitivity of the wave solution with respect to the damping coefficient (Wirth 1991). On the other hand, the effect of the wave breaking parameterization is clearly visible when considering our two diagnostics for the impact of the waves on the mean flow: the scaled EP flux divergence D_F (middle row in Fig. 3) and the residual circulation ψ (lower row in Fig. 3). In Fig. 3d, there appear two distinct maxima of D_F in the middle and upper stratosphere, one on each flank of the polar night jet. A comparison of the two fields of D_F in Fig. 3 with the damping rate δ in Fig. 2b suggests that the equatorward maximum primarily results from the wave breaking parameterization, while the poleward maximum does not. The latter is mostly due to the damping represented by the coefficient α_0. Both the characteristic pattern of the wave forcing D_F and its maximum values around 3–4 m s^{-1} day^{-1} are in good agreement with the climatology of Randel (1992) and with previous modeling studies (Garcia 1991; Kinnersley 1995). Owing to the factors ρ_0 and $\cot\phi$ on the right-hand side of (13), it is mostly the equatorward lower stratospheric features in D_F that determine the strength and the shape of the residual circulation ψ. This explains why, in Fig. 3, the differences arising from the wave breaking parameterization are even more pronounced in terms of ψ than in terms of D_F. When the wave breaking is included, the residual streamfunction indicates forcing of upward motion in the subtropical lower stratosphere and downward motion in the extratropics. This behavior is more consistent with the general picture of the lower stratospheric Brewer–Dobson circulation (Rosenlof and Holton 1993) than the behavior of the model without the wave breaking parameterization. Of course, we do not expect or even claim a precise quantitative representation. One specific model deficiency is the assumption of stationarity implicit in (13), which represents ''downward control'' as a special case of the more general concept of ''nonlocal control.'' On finite timescales, one may expect the residual circulation to extend father poleward from the forcing region, where $D_F \neq 0$ [see section 3 in Holton et al. (1995)].

It is instructive to study the model response to varying the lower boundary forcing Φ'_{TP}. Here we present results only for wavenumber 1, but the results for wavenumber 2 are quite similar. The left row in Fig. 4 shows how the damping coefficient δ is modified when Φ'_{TP} is halved and doubled, respectively, with respect to the January climatology. For weak forcing (panel a), wave breaking is restricted to the middle stratosphere between $z = 30$ and $z = 45$ km. For stronger forcing, the region of wave breaking extends both upward and downward, while the maximum value of δ increases less than linearly with the forcing (see also line B in Fig. 5). The corresponding residual circulation ψ is given in the right column of the same figure, where the contour interval increases by a factor of 4 each time when going from panel (b) over (d) to (f). If α were a constant, q' would be linear in Φ'_{TP}, and $\mathbf{F}$, D_F, and ψ would be quadratic in Φ'_{TP}. With the chosen contour convention, the appearance of the plot would be the same in all three cases. However, the actual appearance of the three plots is quite different, illustrating the nonlinearity inherent in the current model. The stronger the forcing is, the more the contours of ψ are concentrated in the lower stratosphere. This behavior is considered to be realistic: for strong forcing, the attenuation of the wave at lower levels limits the wave activity arriving at higher levels. The dependence of various model parameters on Φ'_{TP} is summarized in Fig. 5. This plot presents the dependencies in such a format that the curves A, C, and D would be identical

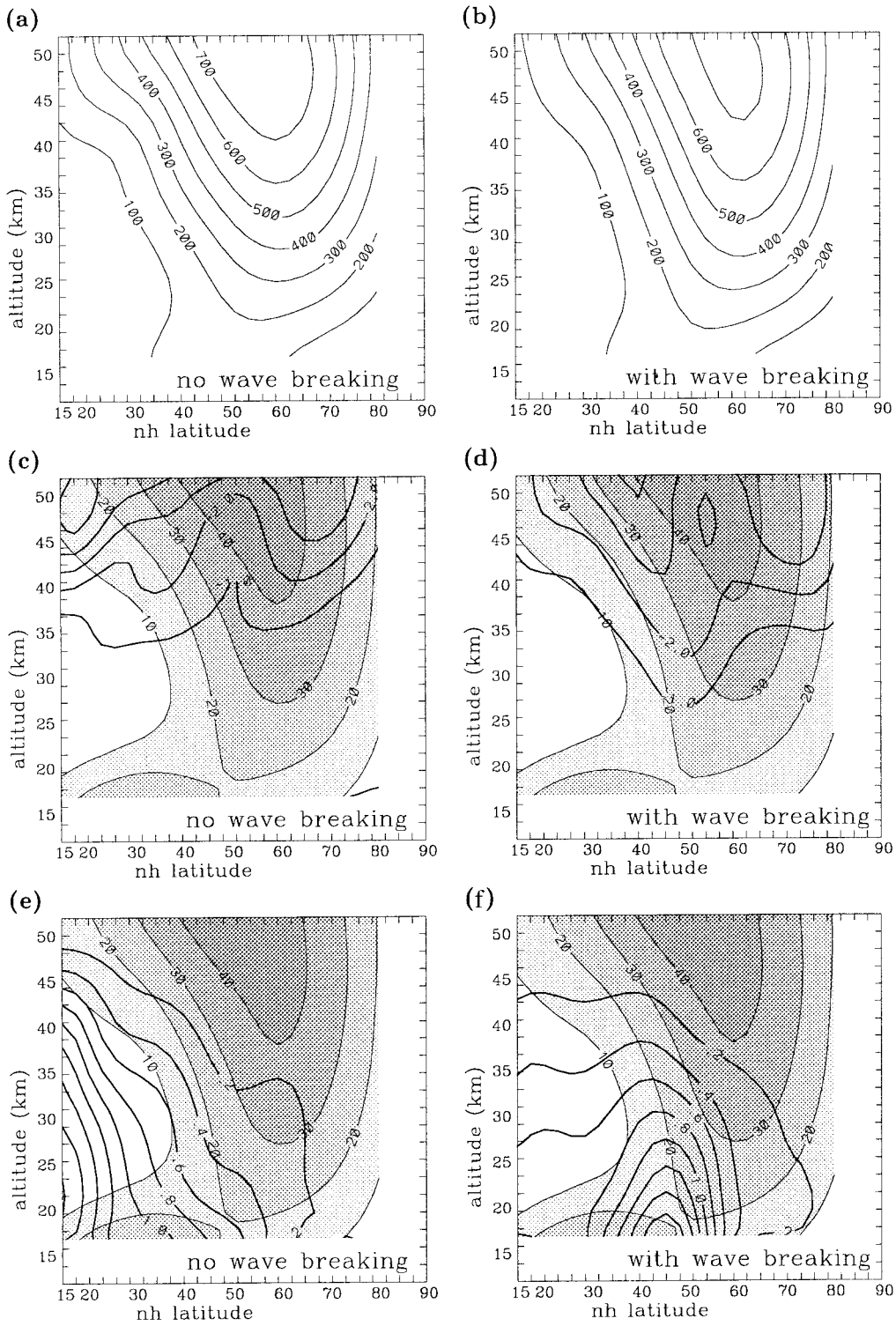

FIG. 3. Model results for wavenumber 1 and the reference basic state, without the wave breaking parameterization (left column) and with the wave breaking parameterization (right column). The upper row shows wave amplitude (in m, contours every 100 m), the middle row shows the scaled EP flux divergence D_F (in m s^{-1} day^{-1}, thick contours every 1 m s^{-1} day^{-1}), and the bottom row depicts the residual streamfunction ψ (in 10^{-7} kg m^{-1} day^{-1}, thick contours every 0.2×10^{-7} kg m^{-1} day^{-1}). The thin contours and shading in (c)–(f) depict the basic state zonal wind (in m s^{-1}, contours every 10 m s^{-1}).

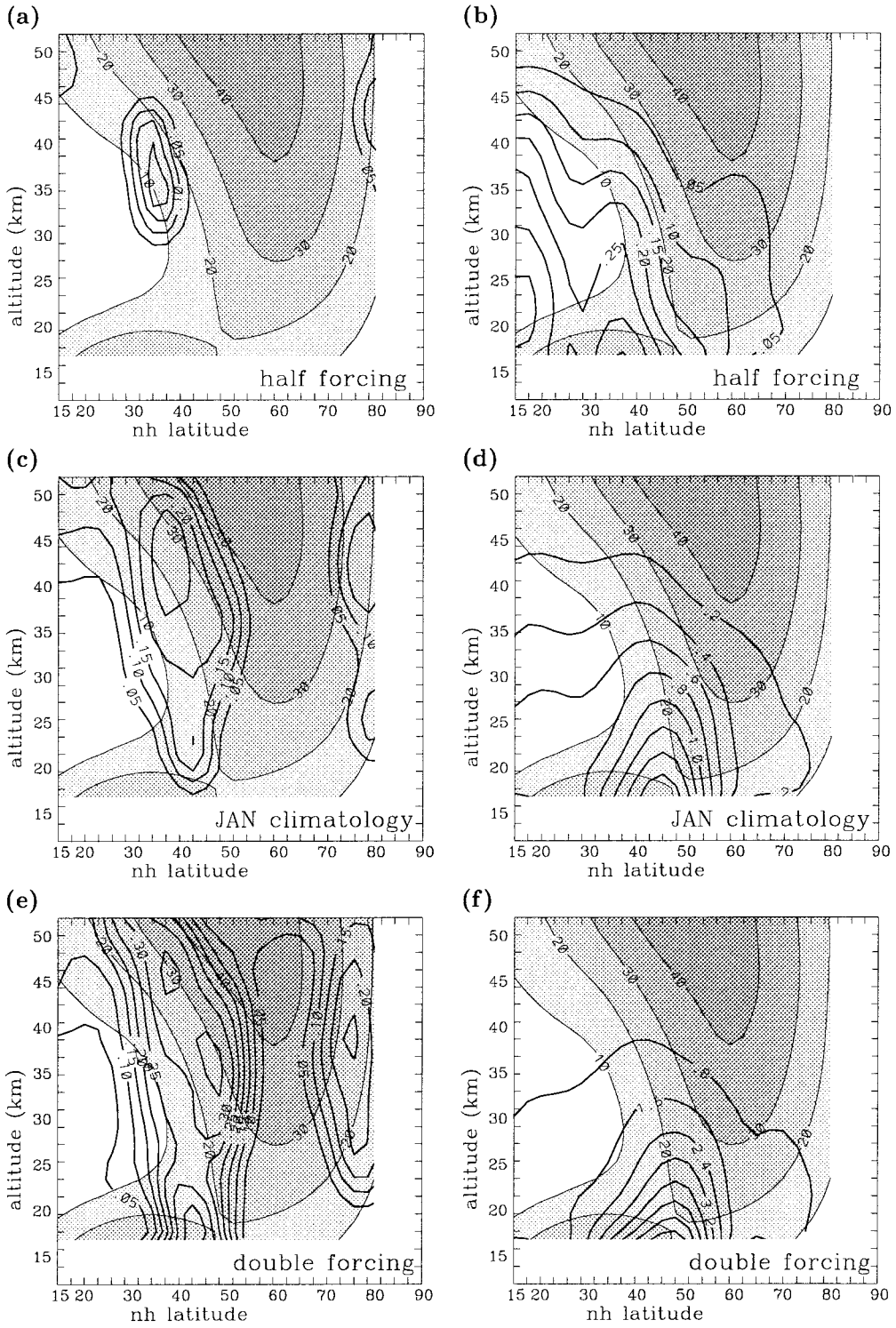

FIG. 4. Model response (wavenumber 1) for different amplitudes of the lower boundary forcing Φ'_{TP}. The middle row depicts the scenario for the Jan climatology, while the top and the bottom rows correspond to halving and doubling, respectively, of this forcing. The left column shows the damping coefficient δ (in day^{-1}, thick contours every 0.05 day^{-1}), while the right column depicts the residual streamfunction ψ [thick contours, in 10^{-7} kg m^{-1} day^{-1}; the contour interval is 0.05×10^{-7} kg m^{-1} day^{-1} in (b), 0.2×10^{-7} kg m^{-1} day^{-1} in (d), and 0.8×10^{-7} kg m^{-1} day^{-1} in (f)]. In all panels, the thin contours and shading represent the basic state zonal wind $\overline{u}$ shown in Fig. 1a.

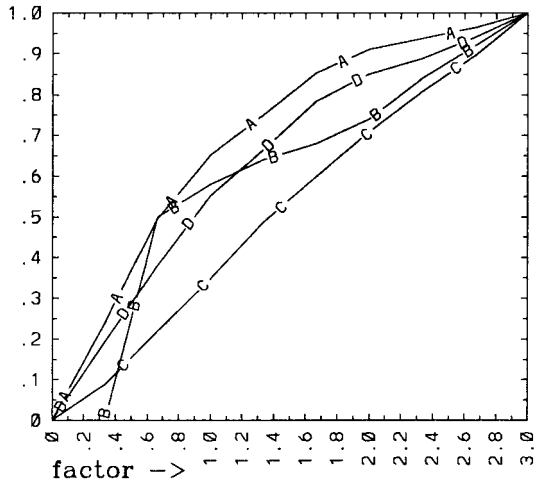

FIG. 5. Model sensitivity to the amplitude of the lower boundary forcing Φ'_{TP} for wavenumber 1. The abscissa denotes the factor $\hat{f}$ by which the climatological value of Φ'_{TP} was multiplied. All function values were computed at $\hat{f} = 0, 0.3, 0.6, \ldots, 3$ with linear interpolation in between; in addition, they are normalized to be equal to 1 at $\hat{f} = 3$. The four lines denote: A = maximum amplitude of geopotential $\Phi'(\phi, z)$, B = maximum value of $\delta(\phi, z)$, C = maximum value of $\sqrt{\psi(\phi, z_0)}$ at $z_0 = 17$ km, and D = maximum value of $\sqrt{\psi(\phi, z_0)}$ at $z_0 = 35$ km. The term "maximum value" corresponds to the region $35°\text{N} \le \phi \le 80°\text{N}$ in latitude and (if it applies) to 17 km $\le z \le$ 53 km.

straight lines in the event of linear damping with constant α. Deviation from such linear behavior is noticeable except for small forcing. Overall, the maximum wave amplitude (curve A) grows less than linearly with Φ'_{TP}, and the residual circulation in the middle stratosphere (curve D) grows less than quadratic in Φ'_{TP}. As mentioned above, this is interpreted as a result of increased wave dissipation in the lower stratosphere for increased forcing Φ'_{TP}, which attenuates the wave, permitting relatively less wave activity to penetrate into the middle and upper stratosphere. On the other hand, the residual streamfunction at the lower boundary is roughly quadratic in Φ'_{TP} rendering curve C in Fig. 5 approximately a straight line.

4. Application

The model is now applied to a situation in which wave–mean-flow interaction is known to play an important role. We consider the relationship between the QBO and the strength of the polar vortex. Such a connection was first noted by Holton and Tan (1980), who observed warm polar temperatures associated with a relatively weak jet during the easterly phase and cold temperatures associated with a strong jet during the westerly phase of the QBO. They proposed that the observed correlations are mediated by a modulation of stratospheric planetary waves. Because of lower latitude easterlies and, hence, a poleward shift of the critical line during the easterly phase, wave propagation should be modified, since the waves tend not to propagate across critical lines or into regions with small basic state PV gradient (Matsuno 1970). At the same time, more wave activity is dissipated at the equatorward flank of the polar night jet, leading to increased wave forcing D_F and a stronger residual circulation, which, in turn, is associated with a weaker polar vortex. On the other hand, during the westerly phase the waves can readily propagate into the subtropics without much dissipation, resulting in a weak residual circulation and leaving the polar vortex undisturbed and strong. This overall picture was confirmed in various subsequent studies (Holton and Tan 1982; Labitzke 1982, 1987; van Loon and Labitzke 1987; Dunkerton and Baldwin 1991; Kodera 1991). Yet, there is still some uncertainty about the precise nature of the mechanisms involved.

In order to represent the change of the basic state due to the QBO in our model, we modify the reference basic state $\overline{u}$ by adding a term $\overline{u}_0 \cos^2\phi$, that is, we introduce

$$\overline{u}^{\text{mod}} = \overline{u} + \overline{u}_0 \cos^2\phi, \tag{14}$$

where $\overline{u}_0$ is a constant wind. With $\overline{u}_0 = +15$ m s^{-1}, the modified basic state $\overline{u}^{\text{mod}}_{+15}$ resembles the westerly phase of the QBO, with westerlies throughout the model domain (Fig. 6a). The easterly phase is simulated by setting $\overline{u}_0 = -15$ m s^{-1}, yielding a basic state $\overline{u}^{\text{mod}}_{-15}$ with easterlies in the lower latitudes and with the critical line reaching as far as 30°N (Fig. 6b). The modification thus leads to significant changes in the lower latitude basic state. On the other hand, the location and strength of the jet maximum are essentially unchanged (cf. Fig. 1). Also, the PV gradient $\overline{q}_\phi$ of the modified basic state (not shown) is practically unaffected and can hardly be distinguished from the pattern for the reference basic state in Fig. 1b. Following Matsuno (1970), we plot the quantity $a^2 n_s^2$ for $s = 0$ in the lower two panels of Fig. 6. Apparently, in terms of n_0^2 the modification shows very clearly as the critical line in the case of QBO east is associated with a singularity of the refractive index. On the other hand, in the jet region and poleward of it the quantity n_0^2 is not strongly affected.

The results for wavenumber 1 are summarized in Fig. 7. There are small but noticeable differences in the wave amplitude (upper row), with the maximum in the upper stratosphere being some 20% stronger and located further poleward for the easterly phase of the QBO. To the degree that the PV gradient $\overline{q}_\phi$ diagnoses the wave amplitude, one would expect practically no difference in wave amplitude, as the two basic states have practically identical $\overline{q}_\phi$ (see above). To the degree that the refractive index sqare n_0^2 indicates wave propagation, the differences in wave amplitude can well be explained by the differences in $a^2 n_0^2$ shown in Fig. 6. However, what is much more interesting in the current context is that the difference between the two QBO phases is much more pronounced in terms of the wave forcing D_F and the residual circulation ψ (middle and bottom row, respectively). The wave forcing D_F is weak in the westerly phase experiment, with maximum values reaching some

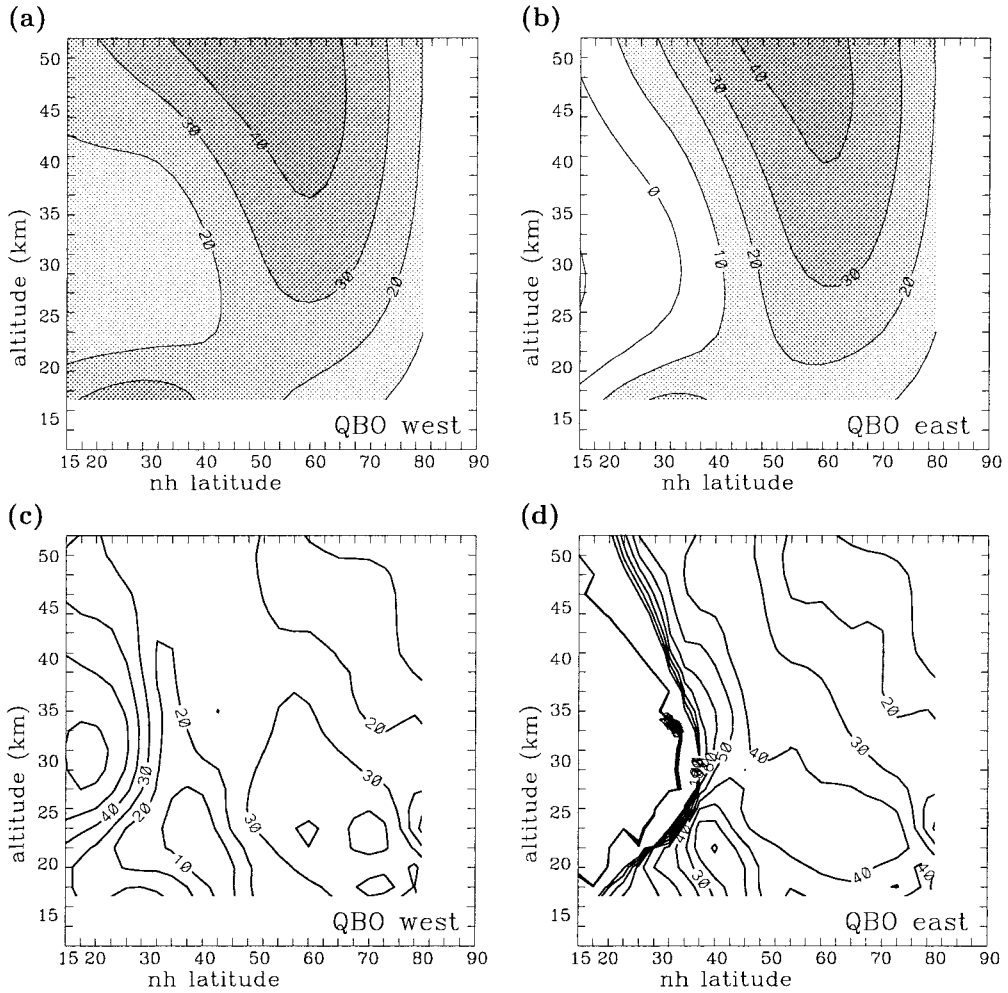

FIG. 6. The two modified basic states for the QBO-simulation, $\overline{u}^{\text{mod}}_{+15}$ (left column) and $\overline{u}^{\text{mod}}_{-15}$ (right column). The two panels in the upper row show the zonal mean zonal wind $\overline{u}$ (in m s^{-1}, contours every 10 m s^{-1}), while the lower two panels show the corresponding refractive index squared $a^2\, n_0^2$ (dimensionless, contours every 10).

$-$ 2 m s^{-1} day^{-1}, which is roughly half the value of the reference run (Fig. 3d). On the other hand, the wave forcing is strong in the easterly phase experiment, reaching values up to $-$ 5 m s^{-1} day^{-1} and covering a broad area on the equatorward flank of the jet maximum. The residual circulation ψ shows the differences even more clearly, with the maximum value being almost three times larger in the case of the QBO east compared with QBO west. Apparently, a simple poleward shift of the critical line in our model produces very substantial differences for the diagnosed wave forcing and residual circulation.

The behavior in our model is qualitatively consistent with the results of Holton and Tan (1980), who noted a significant difference in the temperature of the polar vortex between the two phases of the QBO, while the correlation between the QBO and the wave amplitude was much less pronounced. In our model scenario, the differences between the phases of the QBO are basically due to differences in the location of the critical line. This result is consistent with more recent studies by Balachandran and Rind (1995) and Chen (1996), who found strong sensitivity to the location of the critical line in connection with the QBO using a global circulation model and a high resolution barotropic model, respectively. Holton and Tan found the largest differences between the two phases of the QBO in polar temperatures, while our model seems to indicate the largest differences in downwelling near 55°N. This shortcoming may be due to our assumption of stationarity in equation (13); as mentioned before, accounting for finite timescales would spread the residual circulation more into polar latitudes.

Figure 8 shows the results for wavenumber 2. The corresponding forcing Φ'_{TP} is again taken from Randel (1987). The wave amplitudes range between 100 and 300 meters (upper row), which is less than half of the values for wavenumber 1. The further poleward the critical line is located (cf. shading and thin contours in the middle and bottom row), the more the wave propagation

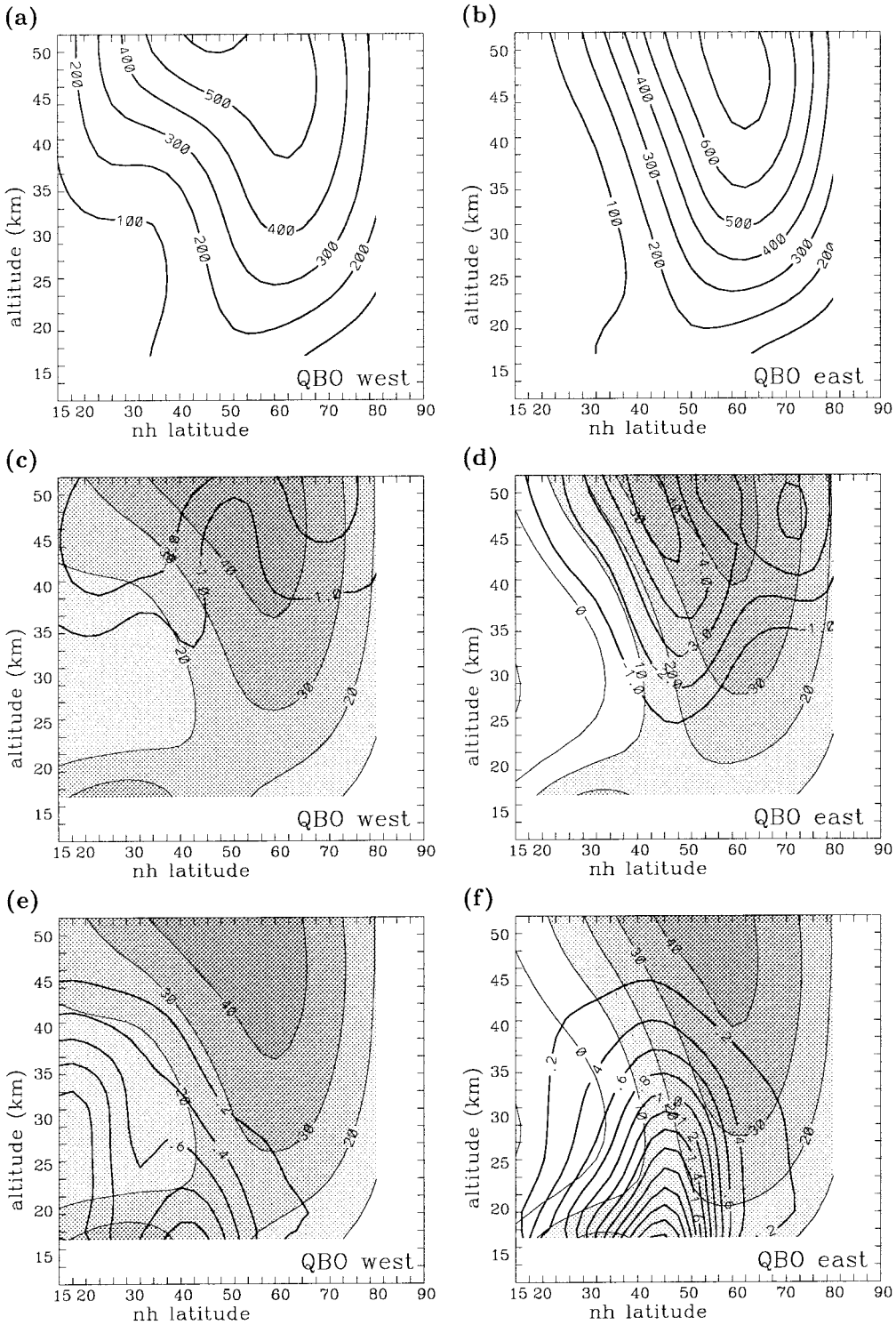

FIG. 7. Model results for wavenumber 1 and the two simulated QBO phases: westerly phase (left column) and easterly phase (right column). The upper row shows wave amplitude (in m, thick contours every 100 m), the middle row shows the scaled EP flux divergence D_F (in m s^{-1} day^{-1}, thick contours every 1 m s^{-1} day^{-1}), and the bottom row depicts the residual streamfunction ψ (in 10^{-7} kg m^{-1} day^{-1}, thick contours every 0.2×10^{-7} kg m^{-1} day^{-1}). The thin contours and shading in (c)–(f) depict the basic state zonal wind (in m s^{-1}, contours every 10 m s^{-1}).

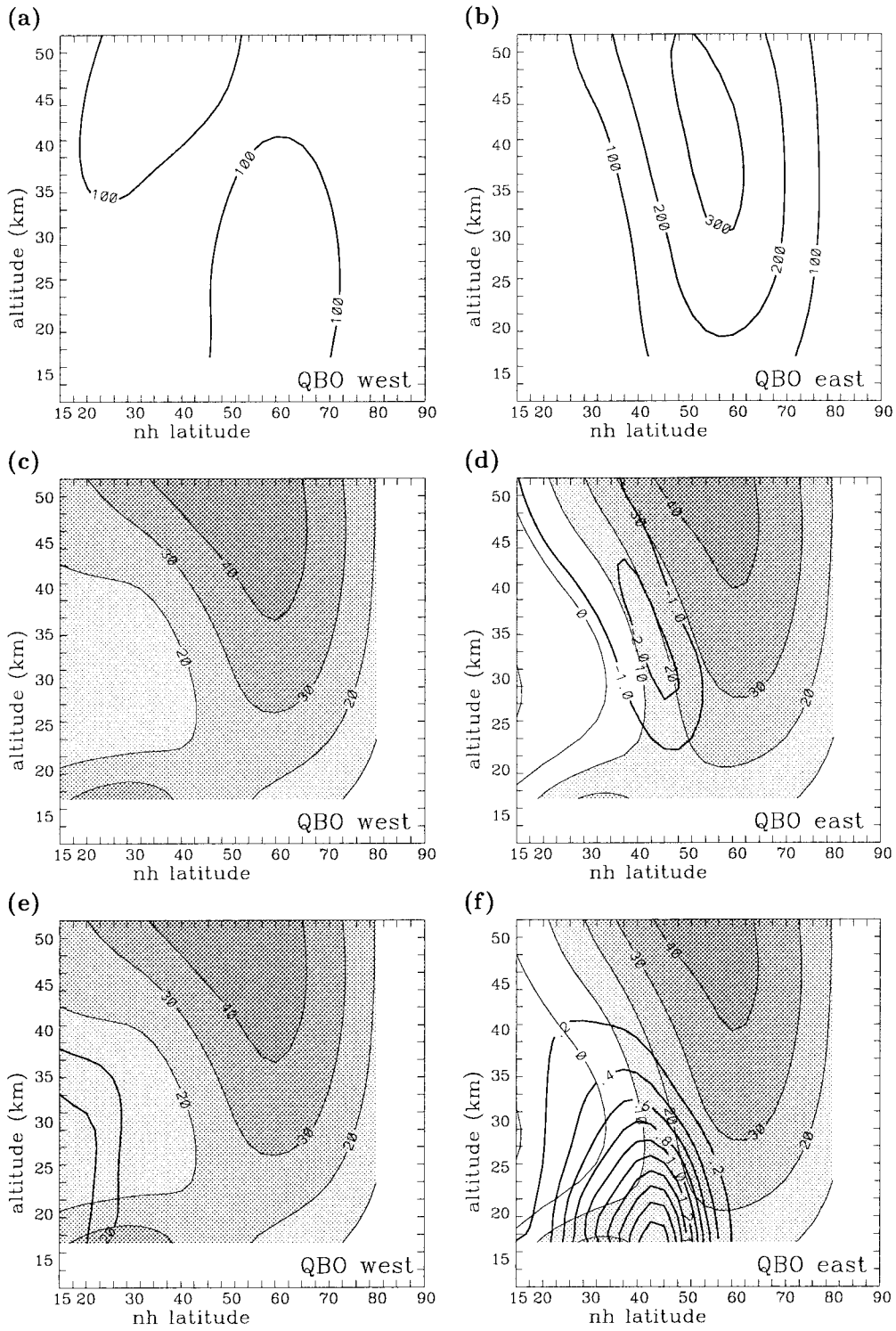

FIG. 8. As Fig. 7 but for wavenumber 2.

seems to be confined to higher latitudes. Again, more pronounced differences show up in terms of wave forcing D_F (middle row) and the residual streamfunction ψ (bottom row). While there is hardly any wave forcing diagnosed for the QBO west phase (no contours for D_F appearing in Fig. 8c), there is substantial wave forcing (up to 2 m s^{-1} day^{-1}) in a broad band along the equatorward flank of the polar vortex throughout the strato-

TABLE 1. Maximum value of the residual streamfunction $\psi(\phi, z_0)$(in 10^{-7} kg m^{-1} day^{-1}) poleward of 40°N at $z_0 = 17$ km. This value can be interpreted as a proxy for the total amount of mass forced downward across the extratropical tropopause. The three rows represent the climatology (middle row) and the two idealized QBO experiments (first and third row), respectively. The two columns refer to wavenumbers 1 and 2 ($s = 1, 2$). In each case, the first table entry represents the experiment with the Rossby wave parameterization switched on, while the second entry (value in parentheses) refers to the corresponding experiment without the parameterization.

	$s = 1$	$s = 2$
QBO west	1.1 (0.6)	0.1 (0.1)
CLIM	1.7 (0.9)	0.8 (0.4)
QBO east	2.6 (1.8)	2.3 (1.4)

sphere in the QBO east experiment (right column). Similarly, the residual streamfunction shows huge differences between the two QBO phases. In the lower stratosphere, the downwelling vertical wind, which is related to the horizontal spacing of the streamlines, is over a factor 10 times stronger for QBO east than for QBO west. Such big differences cannot be merely due to the difference in wave amplitude or wave propagation; they must be related to the different wave dissipation in the subtropics.

It is instructive to compare the wave 2 results for the $\overline{u}^{\text{mod}}_{-15}$ basic state (right column in Fig. 8) with the wave 1 results for the $\overline{u}^{\text{mod}}_{+15}$ basic state (left column in Fig. 7). In both experiments, the wave forcing D_F is similar in magnitude (1–2 m s^{-1} day^{-1}) even though the maximum wave amplitude differs by a factor of 2 (600 vs 300 m). The comparison is even more striking for the residual streamfunction ψ, which has more than double maximum values in the wave 2 experiment compared with the wave 1 experiment (2.1 as opposed to 0.9×10^{-7} kg m^{-1} day^{-1}). Consequently, the impact of the waves on the basic flow is very large in the wavenumber 2 QBO east experiment even though consideration of the wave amplitude alone would suggest the opposite. This somewhat counterintuitive behavior is based on the fact that the EP flux divergence does not only depend on the wave amplitude A_s but also on its phase χ_s [cf. (8) and (9)]. Table 1 summarizes the impact of the Rossby wave breaking parameterization for our idealized QBO experiments. Although the behavior is qualitatively similar for the runs with and without the parameterization, the numbers differ by up to a factor of 2. Moreover, for some of the runs, the residual circulation looks rather awkward when the parameterization is switched off, while its inclusion always leads to a ''reasonable'' pattern.

Our diagnostic results for wavenumber 2 are consistent with the role of wavenumber 2 for major stratospheric warmings (e.g., Labitzke 1981; Palmer 1981a, b; Robinson 1986; Andrews et al. 1987). The strong sensitivity that we found suggests that ''preconditioning'' of the mean flow may affect the polar vortex not only through changed wave propagation and vortex ''erosion'' but also through a strongly enhanced residual circulation. To be sure, vortex erosion and an enhanced residual circulation are intimately related. The new aspect of the current analysis is the strong sensitivity of either process with respect to the basic state.

5. Summary and conclusions

In this paper, a new diagnostic method was presented, which allows us to gain information about the interaction between planetary waves and the mean flow in the context of a linear Matsuno-type model. The essential new element is the implementation of a Rossby wave breaking parameterization developed by Garcia (1991). It yields an improved representation of wave dissipation in the vicinity of the critical lines, where the waves tend to break. From this, we derive the divergence of the EP flux and the streamfunction ψ of the residual circulation associated with wave dissipation on long timescales. This allows one to quantify the wave mean–flow interaction given the basic state zonal wind and the wave at the tropopause level.

The model performance was tested using a Northern Hemisphere January climatology as reference basic state. Wave breaking is diagnosed along the equatorward flank of the polar night jet with realistic damping rates. In contrast to wave amplitude, both the EP flux divergence and the residual circulation sensitively depend on the treatment of the wave damping. A realistic diagnosis of the latter quantities can only be obtained when local wave dissipation due to wave breaking is accounted for. The various model parameters depend in a complex way on the lower boundary forcing Φ'_{TP}. For weak forcing, wave breaking is restricted to the middle stratosphere, while for stronger forcing, the region of wave breaking becomes more extended, and part of the wave activity is dissipated in the lower stratosphere. As a consequence, the residual streamfunction increases overall less rapidly with increasing Φ'_{TP} than what one would obtain for a constant damping coefficient.

We simulated an idealized QBO by suitable modifications to the basic state zonal flow on the equatorward flank of the polar night jet, leaving the meridional potential vorticity gradient $\overline{q}_\phi$ practically unchanged. The resulting wavenumber 1 amplitude differs only slightly for the two phases of the QBO. On the other hand, the two basic states differ substantially in the location of their critical lines and, hence, the amount of diagnosed Rossby wave breaking. As a result, the model diagnoses a much stronger residual streamfunction ψ for the QBO east phase than for the QBO west phase. This is qualitatively in good agreement with the observations of Holton and Tan (1980) and subsequent authors, who found a warm and weak polar vortex during the easterly phase but a cold and stable vortex during the westerly phase of the QBO. Our result emphasizes the key diagnostic role of the EP flux divergence, which depends much more sensitively on the differences in the basic

state than either the wave amplitude or the EP flux itself (cf. Braesicke 1994). A similar set of experiments for wave 2 corroborated the usefulness of our diagnostics.

Overall, our results suggest that in a linear Matsuno-type model, neither the wave amplitude nor the EP flux **F** is a good indicator for the impact of Rossby waves on the mean flow. In certain cases, large amplitude waves may propagate through the entire stratosphere without substantial interaction. In other cases, small amplitude waves may get strongly dissipated, leading to a large wave forcing D_F and a strong residual circulation ψ. Without explicit accounting for wave breaking, these crucial differences between wave propagation and wave dissipation are not correctly represented in the context of Matsuno's model.

Because of the qualitative agreement of our idealized QBO results with the results from previous investigations, we believe that the application of the new diagnostic will be fruitful in other situations that are less well understood. For instance, it should be interesting to investigate the presumed impact of the 11-yr solar cycle on the stratospheric circulation and the interaction between the solar cycle and the QBO (Labitzke and van Loon 1988; Kodera 1991; Dunkerton and Baldwin 1992). This problem was investigated by Braesicke (1994) using the standard Matsuno model. He mainly analyzed the EP flux **F** showing that different prototypical basic states affect the wave amplitude and wave propagation in different ways. In the end, his results appeared somewhat inconclusive. We think that this is not too surprising, because one should analyze $D_F \propto \nabla \cdot \mathbf{F}$ or the associated residual circulation ψ, rather than **F** itself. In addition, more recent research has shown that the four basic states analyzed by Braesicke are possibly not the most relevant ones (Kodera 1993, 1995). We anticipate that our model can throw new light on this issue, but this would require more detailed work and transcends the scope of the present paper.

In summary, we proposed a new method that allows one to diagnose the impact of stratospheric planetary waves on a given mean flow resulting from wave dissipation and, especially, wave breaking. We demonstrated that the method is able to reproduce essential features in a situation that has been thoroughly studied in the past. Our results suggest that the application to other problems will help to disentangle the different dynamical processes existing in complex numerical models and in the real atmosphere.

Acknowledgments. We would like to thank J. Egger and three anonymous referees for constructive criticism on an earlier version of this paper.

APPENDIX

Convergence of the Solution

In order to determine the convergence of the solution in the context of our iterative technique, we consider a global norm for D_F, since this is the quantity we are eventually interested in. Unfortunately, the iteration does not converge in a strict mathematical sense. This is not too surprising, since D_F sentivitely depends on δ, which in turn is a discontinous function in the meridional plane owing to the wave breaking criterion (5). Nevertheless, following large changes during the first few iterations, the norm always reaches a finite oscillation, whose amplitude is much smaller than the large changes initially. We, therefore, take the average δ over one such final oscillation as the solution of the iteration. Sensitivity studies showed that the results are insensitive to the precise way of the averaging. The maximum number of iterations necessary was always less than 50, but in cases with little wave breaking it was considerably smaller. Further sensitivity studies using slightly different convergence criteria gave qualitatively the same results.

REFERENCES

Andrews, D. G., and M. E. McIntyre, 1976: Planetary waves in horizontal and vertical shear: The generalized Eliassen-Palm relation and the mean zonal acceleration. *J. Atmos. Sci.,* **33,** 2031–2048.

——, and ——, 1978: Generalized Eliassen-Palm and Charney-Drazin theorems for waves on axisymmetric mean flows in compressible atmospheres. *J. Atmos. Sci.,* **35,** 175–185.

——, J. R. Holton, and C. B. Leovy, 1987: *Middle Atmosphere Dynamics.* Academic Press, 489 pp.

Balachandran, N. K., and D. Rind, 1995: Modeling the effects of UV variability and the QBO on the troposphere-stratosphere system. Part I: The middle atmosphere. *J. Climate,* **8,** 2058–2079.

Braesicke, P., 1994: Linear wave propagation in the stratosphere: The influence of the mean state. *Beitr. Phys. Atmos.,* **67,** 209–217.

Charney, J. G., and P. G. Drazin, 1961: Propagation of planetary-scale disturbances from the lower into the upper atmosphere. *J. Geophys. Res.,* **66,** 83–109.

Chen, P., 1996: The influences of zonal flow on wave breaking and tropical–extratropical interaction in the lower stratosphere. *J. Atmos. Sci.,* **53,** 2379–2392.

Dunkerton, T. J., and M. P. Baldwin, 1991: Quasi-biennial modulation of planetary-wave fluxes in the northern hemisphere winter. *J. Atmos. Sci.,* **48,** 1043–1061.

——, and ——, 1992: Modes of interannual variability in the stratosphere. *Geophys. Res. Lett.,* **19,** 49–52.

Garcia, R. R., 1991: Parameterization of planetary wave breaking in the middle atmosphere. *J. Atmos. Sci.,* **48,** 1405–1419.

Haynes, P. H., C. J. Marks, M. E. McIntyre, T. G. Shepherd, and K. P. Shine, 1991: On the ''downward control'' of extratropical diabatic circulations by eddy-induced mean zonal forces. *J. Atmos. Sci.,* **48,** 651–678.

Holton, J. R., and H.-C. Tan, 1980: The influence of the equatorial quasi-biennial oscillation on the global circulation at 50 mb. *J. Atmos. Sci.,* **37,** 2200–2208.

——, and ——, 1982: The quasi-biennial oscillation in the Northern Hemisphere lower stratosphere. *J. Meteor. Soc. Japan,* **60,** 140–147.

——, P. H. Haynes, M. E. McIntyre, A. R. Douglass, R. B. Rood, and L. Pfister, 1995: Stratosphere–troposphere exchange. *Rev. Geophys.,* **33,** 403–439.

Karoly, D. J., and B. J. Hoskins, 1982: Three dimensional propagation of planetary waves. *J. Meteor. Soc. Japan,* **60,** 109–123.

Kinnersley, J. S., 1995: A realistic three-component planetary wave model, with a wave-breaking parametrization. *Quart. J. Roy. Meteor. Soc.,* **121,** 853–881.

Kodera, K., 1991: The solar and equatorial QBO influences on the stratospheric circulation during the early Northern Hemisphere winter. *Geophys. Res. Lett.,* **18,** 1023–1026.

——, 1993: Quasi-decadal modulation of the influence of the equatorial quasi-biennial oscillation on the north polar stratospheric temperatures. *J. Geophys. Res.,* **98,** 7245–7250.

——, 1995: On the origin and nature of the interannual variability of the winter stratospheric circulation in the northern hemisphere. *J. Geophys. Res.,* **100,** 14 077–14 087.

Labitzke, K., 1981: The amplification of height wave 1 in January 1979: A characteristic precondition for the major warming in February. *Mon. Wea. Rev.,* **109,** 983–989.

——, 1982: On the interannual variability of the middle stratosphere during the northern winters. *J. Meteor. Soc. Japan,* **60,** 124–139.

——, 1987: Sunspots, the QBO, and the stratospheric temperature in the north polar region. *Geophys. Res. Lett.,* **14,** 535–537.

——, and H. van Loon, 1988: Associations between the 11-year solar cycle, the QBO and the atmosphere. Part I: The troposphere and stratosphere in the Northern Hemisphere winter. *J. Atmos. Terr. Phys.,* **54,** 1453–1463.

Lindzen, R. S., 1981: Turbulence and stress owing to gravity wave and tidal break down. *J. Geophys. Res.,* **86,** 9707–9714.

——, and H.-L. Kuo, 1969: A reliable method for the numerical integration of a large class of ordinary and partial differential equations. *Mon. Wea. Rev.,* **97,** 732–734.

Matsuno, T., 1970: Vertical propagation of stationary planetary waves in the winter Northern Hemisphere. *J. Atmos. Sci.,* **27,** 871–883.

——, 1971: A dynamical model of the stratospheric sudden warming. *J. Atmos. Sci.,* **28,** 1479–1494.

McIntyre, M. E., and T. N. Palmer, 1984: The 'surf zone' in the stratosphere. *J. Atmos. Terr. Phys.,* **46,** 825–849.

Palmer, T. N., 1981a: Diagnostic study of a wavenumber-2 stratospheric sudden warming in a transformed Eulerian-mean formalism. *J. Atmos. Sci.,* **38,** 844–855.

——, 1981b: Aspects of stratospheric sudden warmings studied from a transformed Eulerian-mean viewpoint. *J. Geophys. Res.,* **86,** 9679–9687.

Randel, W. J., 1987: Global atmospheric circulation statistics, 1000-1 mb. NCAR Tech. Note, NCAR/TN-295+STR.

——, 1992: Global atmospheric circulation statistics, 1000-1 mb. NCAR Tech. Note, NCAR/TN-366+STR.

——, and R. R. Garcia, 1994: Application of a planetary wave breaking parameterization to stratospheric circulation statistics. *J. Atmos. Sci.,* **51,** 1157–1168.

Robinson, W. A., 1986: The behavior of planetary wave 2 in preconditioned zonal flows. *J. Atmos. Sci.,* **43,** 3109–3121.

Rosenlof, K. H., and J. R. Holton, 1993: Estimates of the stratospheric residual circulation using the downward control principle. *J. Geophys. Res.,* **98,** 10 465–10 479.

van Loon, H., and K. Labitzke, 1987: The Southern Oscillation. Part V: The anomalies in the lower stratosphere of the Northern Hemisphere in winter and a comparison with the Quasi-Biennial Oscillation. *Mon. Wea. Rev.,* **115,** 357–369.

Wirth, V., 1991: What causes the seasonal cycle of stationary waves in the southern stratosphere? *J. Atmos. Sci.,* **48,** 1194–1200.